Comparative study of the radius of sensitivity of the optical model potentials for ^{6}Li+^{58,64}Ni and ^{16}O+^{58,64}Ni

Mili Biswas*
Saha Institute of Nuclear Physics, 1/AF, Bidhan Nagar, Kolkata-700 064, India
(Received 24 April 2007; revised manuscript received 14 November 2007; published 22 January 2008)

Radii of sensitivity were estimated for the ^{6}Li+^{58,64}Ni system at energies near the Coulomb barrier. For comparison purposes, such radii were also estimated for stable ^{16}O scattered from the same target isotopes. The elastic scattering data were analyzed with folded real potential generated from DDM3Y nucleon-nucleon interaction and an imaginary potential of volume Woods-Saxon form. The most sensitive radii for the ^{16}O+^{58,64}Ni system are found to be energy independent and close to the strong absorption radius. For the ^{6}Li projectile, unlike its strongly bound counterpart, the crossing radius increases with decreasing energy. However, no two crossing situation has been observed for either the ^{6}Li+^{58,64}Ni or the ^{16}O+^{58,64}Ni system at the top of the barrier.

DOI: 10.1103/PhysRevC.77.017602 PACS number(s): 25.60.Bx, 24.10.Ht, 27.20.+n

The threshold anomaly is a well-known phenomenon observed in heavy-ion scattering systems [1] at low bombarding energies. It refers to a strong variation of the real interaction potential with incident energies close to the Coulomb barrier. It is connected with the increasing strength of the imaginary potential corresponding to the increasing availability of local energy to excite reaction channels in the same energy domain. The connection is through a dispersion relation [2,3] that arises from the causality in heavy-ion collisions. The dispersion integral involves the real and imaginary components that need to be evaluated at a certain radius value while investigating the energy dependence of the polarization potentials. The general convention is to evaluate these quantities at the strong absorption radius. However, the question is whether the so-called strong absorption radius corroborates with the most sensitive radius as the bombarding energy decreases. Roubos *et al*. [4] have recently studied the scattering of ^{6}Li and ^{16}O from the heavy mass target ^{208}Pb to investigate the radius of sensitivity for these systems. The authors observed that for tightly bound systems, the appropriate radius of evaluation of dispersion relation is the strong absorption radius; but for weakly bound systems, that is not the case. It is therefore important to ascertain the radial region of sensitivity of the potentials before making use of the dispersion relation. Work has also been carried out in this direction in Refs. [5–8]. In this context, we present a systematic study of the elastic data of ^{6}Li and ^{16}O projectiles on two different isotopes of the medium mass Ni target to determine the radial region of the potential sensitivity and to identify the difference in observation for the weakly and strongly bound natures of the projectile as the target mass decreases.

The elastic angular distributions of the system ^{6}Li+^{64}Ni have been measured in an experiment performed at Bhabha Atomic Research Centre (BARC)-Tata Institute of Fundamental Research (TIFR) in Mumbai, India, using the BARC-TIFR Pelletron facility over the energy range 13–26 MeV [9]. We have reanalyzed the existing data for the system ^{6}Li+^{58}Ni [10]. For the ^{16}O+^{58,64}Ni system, we used the data of Refs. [5,11]. Figures 1 and 2 show the elastic angular distributions at some of the energies.

To investigate the radius of potential sensitivity and its possible variation with incident energy, we analyzed the 12, 14, 16, 18, and 20 MeV data of ^{6}Li+^{58}Ni, and 13, 14, 17, 19, and 26 MeV data of ^{6}Li+^{64}Ni. The plots for the crossing point radii at 14, 19, and 26 MeV for ^{6}Li+^{64}Ni are shown in Fig. 3. For comparison, the same plots at 44 and 60 MeV for ^{16}O+^{64}Ni are shown in Fig. 4. All the new and existing elastic scattering data were analyzed consistently in terms of the optical model potential. The model potential $U_{\rm mod}(r)$ in the present study has the form

$$U_{\rm mod}(r) = \lambda_r V_{\rm fold}(r) + i W_v(W_0, r_w, a_w; r). \qquad (1)$$

$V_{\rm fold}(r)$ is the double-folded potential and W_v is the imaginary volume Woods-Saxon potential. The renormalization factor λ_r simulates the effect of ΔV, the real part of the polarization potential related to the imaginary component as

$$\Delta V(r; E) = \frac{P}{\pi} \int \frac{W(r; E')}{E' - E}\, dE', \qquad (2)$$

where P denotes the principal value.

The double-folded potentials were calculated with the nickel mass densities obtained from Ref. [13] and the ^{6}Li density by unfolding the parametrized charge density from Ref. [14]. The neutron density of ^{6}Li was assumed to have the same shape as the proton density. Density of ^{16}O was again taken from Ref. [13]. The M3Y nucleon-nucleon interaction in DDM3Y [15,16] convention was used for the calculation that includes an intrinsic energy dependence through a multiplicative factor of $g(E) = (1–0.002E)$.

To obtain the best fit parameters of the potentials, the analysis was started with the highest energy data for all the systems. At the highest energy, we performed an initial search over all the four parameters $(\lambda_r, W_0, r_w, a_w)$ of the model potential $U_{\rm mod}(r)$. Subsequently, the imaginary radius parameter obtained from the initial search was kept fixed. The best fit, determined by χ^2 minimization, was found by searching over the real renormalization factor and the imaginary strength while gridding over the imaginary diffuseness a_w. The same search procedure was adopted for all the incident energies. The

*mili.biswas@saha.ac.in

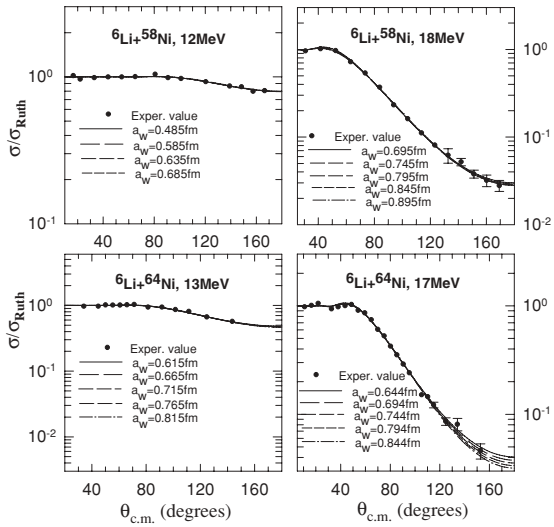

FIG. 1. Elastic scattering angular distributions for the system ^{6}Li+^{58,64}Ni.

radius parameter was held fixed throughout assuming that the change in the value of r_w due to change in incident energy was not so significant. The range of the diffusivity parameter was determined by the condition of similar χ^2/N. For the systems ^{6}Li+^{58,64}Ni, we considered sets of potential parameters generating equally good fit to the elastic scattering angular distributions shown in Fig. 1 with different diffusivities.

We observed that if we varied the diffusivities beyond the range of values shown, the resultant potentials would not intersect, thus proving that they are not good potentials for properly describing the elastic scattering angular distributions. The same procedure was performed for the system ^{16}O+^{58,64}Ni. In Fig. 2, all the calculated angular distributions with different diffusivities are shown. Though the χ^2/N values of the fits vary within the range of $2\chi^2_{\min}/N$, the corresponding fits are quite good. The observed departure at large angles are well within the error limit of the data. For these systems, the crossing points are close to the strong absorption radius where

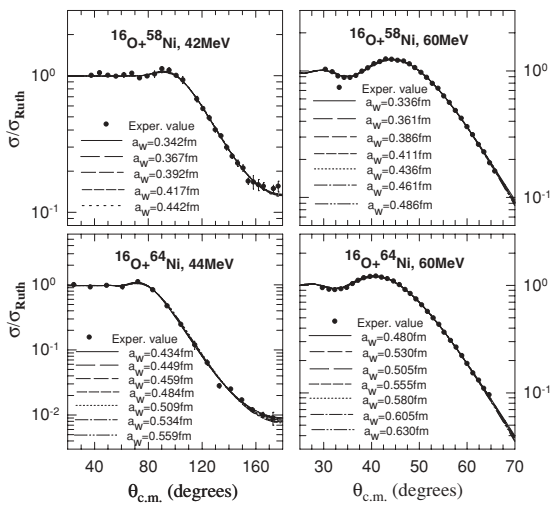

FIG. 2. Elastic scattering angular distributions for the system ^{16}O+^{58,64}Ni.

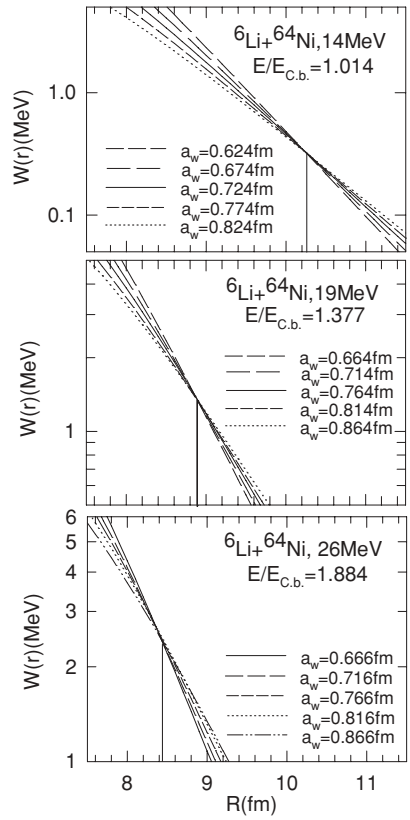

FIG. 3. Crossing radii for the system ^{6}Li+^{64}Ni at different energies. Coulomb barrier is 13.8 MeV in the laboratory frame according to Broglia and Winther [12].

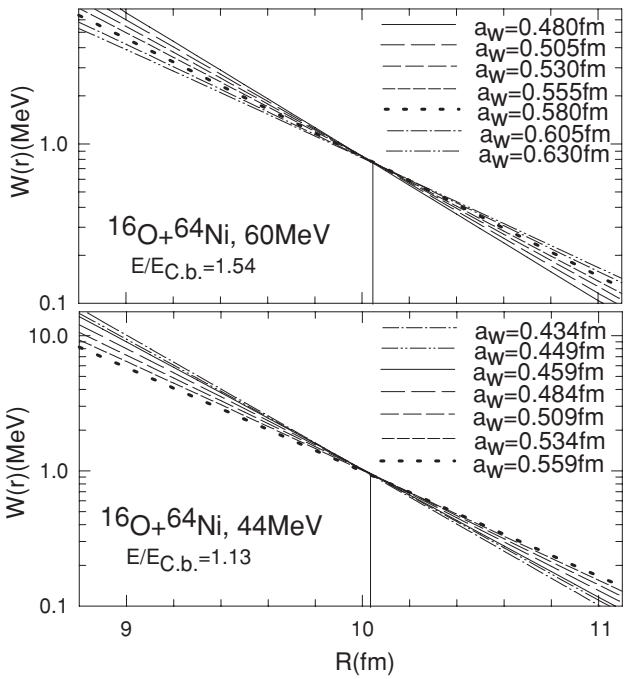

FIG. 4. Crossing radii for the system ^{16}O+^{64}Ni; in the laboratory frame, $E_{\text{C.b.}} = 38.85$ MeV [12].

TABLE I. Potential parameters for ^{6}Li+^{64}Ni.

E(MeV)	N_R	WS	R_w	a_w	χ^2/point	σ_R(mb)
14.0	0.97	87.90	6.753	0.624	4.161	362.73
	0.85	58.52	6.753	0.674	4.065	365.54
	0.75	41.13	6.753	0.724	4.036	369.59
	0.67	29.95	6.753	0.774	4.063	374.60
	0.60	22.71	6.753	0.824	4.155	379.22
19.0	0.65	34.93	6.753	0.664	3.236	913.89
	0.58	28.15	6.753	0.714	3.107	932.22
	0.51	23.56	6.753	0.764	3.091	953.11
	0.44	19.81	6.753	0.814	3.192	972.34
	0.38	17.29	6.753	0.864	3.431	997.94
26.0	0.72	32.58	6.753	0.666	0.633	1401.56
	0.67	27.70	6.753	0.716	0.574	1431.90
	0.60	24.46	6.753	0.766	0.536	1467.47
	0.53	21.87	6.753	0.816	0.522	1504.00
	0.45	19.31	6.753	0.866	0.522	1535.46

the various reactions are expected to take place. The search code ECIS94 [17] was used to perform the model calculations. The optical model potential parameters obtained following the above search procedure along with the χ^2/N (N denotes the number of data points) values and the reaction cross sections σ_R with different diffusivities are given in Tables I and II.

Note that with the chosen model potential, our search procedure will only provide the crossing point for the imaginary potential. No crossing will be observed in the real potentials as the shapes and falloff of these potentials are pre-fixed. Therefore, the crossing point of the imaginary potentials will be treated as the radius of potential sensitivity. It is evident from the figures that the imaginary crossings are quite distinct and unambiguous for these systems at all the energies studied.

The observed phenomenon is that at near barrier energies, the tightly bound projectiles such as ^{16}O, in principle, probe a unique radius of the potential determined by the crossing point radius, and it is very close to the strong absorption radius. The variation of crossing point radius or sensitive radius with incident energy is not significant. Therefore the evaluation of the dispersion integral at the strong absorption radius is quite justified. For the weekly bound projectiles, the behavior is different. The crossings for ^{6}Li+^{58,64}Ni are located in the vicinity of the strong absorption radius for higher bombarding energies, but the values are larger by ∼20% than the strong absorption radius at lower bombarding energy. Similar observation for light targets has also been reported by Roubos *et al.* [4]. Hence care should be taken while evaluating the dispersion relation in the investigation of energy dependence of effective potential for loosely bound projectiles. The crossing radii obtained for ^{6}Li+^{64}Ni and ^{16}O+^{64}Ni are compared in Table III.

TABLE III. Crossing radii with energy for ^{6}Li+^{64}Ni and ^{16}O+^{64}Ni.

E (MeV)	Radius (fm) for ^{6}Li+^{64}Ni	E (MeV)	Radius (fm) for ^{16}O+^{64}Ni
13.0	10.80	44.0	10.10
14.0	10.25	60.0	10.05
17.0	9.60		
19.0	8.90		
26.0	8.43		

An interesting aspect of the work in Ref. [4] is the observation of two crossing points below or at the top of the barrier energies for the ^{6}Li+^{208}Pb and ^{16}O+^{208}Pb systems. The authors have shown that the one at the higher radius value corresponds to nearside scattering and the other at the lower radius value corresponds to farside scattering. To identify the crossings associated with nearside and farside scattering, we followed the prescriptions of Ref. [4]. We have performed our analysis in two steps for all the four systems at top of the barrier energies. First, we fitted our elastic angular distributions considering the forward angle data only, that is, $15^\circ \leqslant \theta_{\mathrm{c.m.}} \leqslant 125^\circ$ angles, up to the point where the ratio of the angular distribution to Rutherford drops to ∼0.5. Next, we took into account only the backward angle data, more specifically, $123^\circ \leqslant \theta_{\mathrm{c.m.}} \leqslant 176^\circ$, to obtain the fit. We did not observe the "two crossings" situation for either the ^{6}Li+^{58,64}Ni

TABLE II. Potential parameters for ^{16}O+^{64}Ni.

E (MeV)	N_R	WS	R_w	a_w	NORM	χ^2/point	σ_R (mb)
44.0	1.41	1452.50	6.846	0.434	0.976	1.248	500.95
	1.37	1150.60	6.846	0.449	0.976	1.418	504.03
	1.34	990.78	6.846	0.459	0.976	1.564	505.95
	1.27	694.80	6.846	0.484	0.976	2.031	510.40
	1.20	501.50	6.846	0.509	0.976	2.625	515.04
	1.14	370.60	6.846	0.534	0.976	3.329	519.43
	1.08	280.27	6.846	0.559	0.976	4.133	523.67
60.0	1.26	597.10	6.846	0.480	1.001	4.522	1208.94
	1.22	433.30	6.846	0.505	1.001	3.424	1215.79
	1.18	323.30	6.846	0.530	1.001	2.756	1222.59
	1.15	246.40	6.846	0.555	1.001	2.531	1229.16
	1.11	192.35	6.846	0.580	1.001	2.769	1235.80
	1.08	152.33	6.846	0.605	1.001	3.490	1242.00
	1.05	122.99	6.846	0.630	1.001	4.706	1248.57

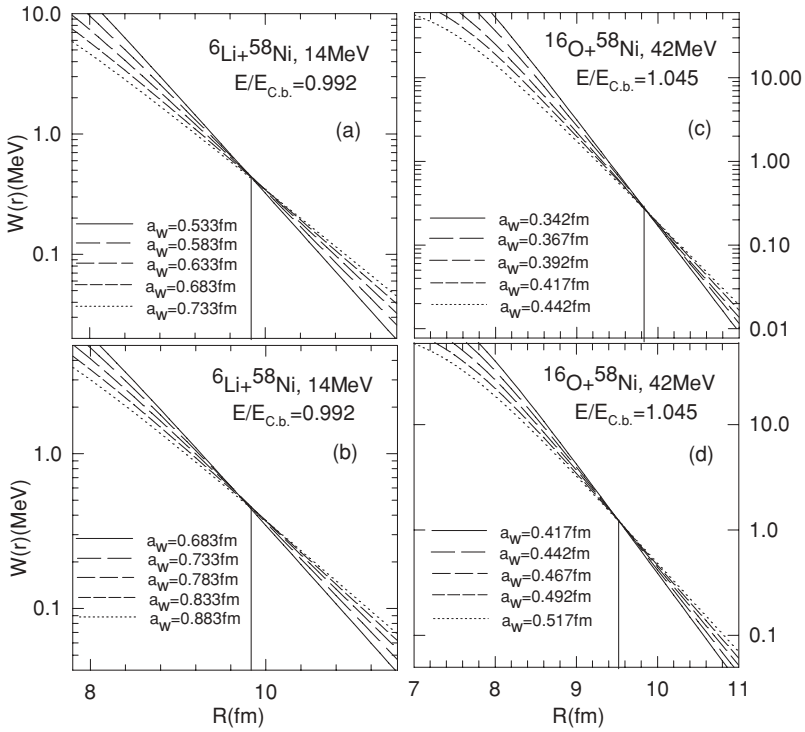

FIG. 5. Crossing points obtained from fits to the forward angle data ($15^\circ \leqslant \theta_{\text{c.m.}} \leqslant 125^\circ$) [(a) and (c)] and backward angle data ($123^\circ \leqslant \theta_{\text{c.m.}} \leqslant 176^\circ$) [(b) and (d)] of the elastic angular distributions of ^{6}Li+^{58}Ni and ^{16}O+^{58}Ni.

or the ^{16}O+^{58,64}Ni system at near barrier energies. In Fig. 5, the crossings associated with two different angular regions of the angular distributions for ^{6}Li+^{58}Ni and ^{16}O+^{58}Ni at near Coulomb barrier energies are compared. The observed crossings for forward and backward angle data differ slightly but not enough to be identified as two distinct crossings. Possibly, the said decoupling between the nearside and farside scattering did not occur at this mass region.

The energy-dependent nature of the crossing point radius for weakly bound ^{6}Li+^{58,64}Ni systems has been depicted in Fig. 3, which shows the crossing radii for ^{6}Li+^{64}Ni at 14, 19, and 26 MeV. As the energy goes higher, the radius becomes smaller with enhanced absorption strength. The same energy dependence has also been observed in the ^{6}Li+^{58}Ni system. Interestingly, these crossing radii are closer to the interaction distances at which the ratio $\sigma/\sigma_{\text{Ruth}}$ for those energies drops to 98%. This possibly indicates that unlike the strongly bound projectiles where fusion at relatively lower radius dominates the absorption process at near barrier energies, the absorption for a loosely bound projectile such as ^{6}Li is dominated by reactions at large separation. Breakup at large separation or single neutron transfer leading to unbound ejectiles could be the possible reaction processes controlling the absorption on approaching the barrier.

In summary, we have performed a systematic radial sensitivity analysis of ^{16}O+^{58,64}Ni and ^{6}Li+^{58,64}Ni elastic scattering data. The two-crossing effect at the barrier has not been observed for any of the four systems studied. However, as pointed out by Roubos *et al.* [4], to probe the existence of two crossings requires more experiments emphasizing the backward angle data with good statistics in the light mass targets.

The author thanks Prof. Subinit Roy for his fruitful discussions and generous help in carrying out this work. In addition, the author gratefully acknowledges N. Keeley for providing the ^{16}O+^{58,64}Ni data in tabular form.

[1] G. R. Satchler, Phys. Rep. **199**, 147 (1991).
[2] C. Mahaux, H. Ngo, and G. R. Satchler, Nucl. Phys. **A449**, 354 (1986).
[3] M. A. Nagarajan, C. C. Mahaux, and G. R. Satchler, Phys. Rev. Lett. **54**, 1136 (1985).
[4] D. Roubos, A. Pakou, N. Alamanos, and K. Rusek, Phys. Rev. C **73**, 051603(R) (2006).
[5] N. Keeley, J. A. Christley, N. M. Clarke, B. R. Fulton, J. S. Lilley, M. A. Nagarajan, and I. J. Thompson, Nucl. Phys. **A582**, 314 (1995).
[6] A. Pakou and K. Rusek, Phys. Rev. C **69**, 057602 (2004).
[7] M. E. Brandan *et al.*, Phys. Rev. C **48**, 1147 (1993).
[8] C. Tenreiro *et al.*, Phys. Rev. C **53**, 2870 (1996).
[9] M. Biswas, M. Sinha, M. Pradhan, P. Basu, H. Majumdar, A. Mukherjee, Subinit Roy, K. Ramachandran, and A. Shrivastava, DAE-BRNS Symp. Nucl. Phys. **50**, 307 (2005).
[10] K. O. Pfeiffer, E. Speth, and K. Bethge, Nucl. Phys. **A206**, 545 (1973).
[11] L. West and N. R. Fletcher, Phys. Rev. C **15**, 2052 (1977).
[12] Ricardo A. Broglia and Aage Winther, *Heavy Ion Reactions, Vol. I, Elastic and Inelastic Reactions* (Benjamin-Cummings, Redwood City, CA, 1981).
[13] http://www-nds.iaea.org/RIPL-2.
[14] G. R. Satchler and W. G. Love, Phys. Rep. **55**, 183 (1979).
[15] D. T. Khoa and W. von Oertzen, Phys. Lett. **B342**, 6 (1995).
[16] A. M. Kobos, B. A. Brown, P. E. Hodgson, G. R. Satchler, and A. Budzanowski, Nucl. Phys. **A384**, 65 (1982).
[17] J. Raynal, ECIS94, NEA 0850/16 (unpublished).